Urban Climate 37 (2021) 100863

Contents lists available at ScienceDirect

Urban Climate

journal homepage: www.elsevier.com/locate/uclim

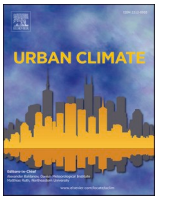

Abating heat waves in a coastal Mediterranean city: What can cool roofs and vegetation contribute?

Joan Gilabert [a,c,d], Sergi Ventura [a], Ricard Segura [a], Alberto Martilli [b], Alba Badia [a], Carme Llasat [c], Jordi Corbera [d], Gara Villalba [a,e,*]

[a] Sostenipra Research Group (SGR 01412), Institute of Environmental Science and Technology (MDM-2015-0552), Z Building, Universitat Autònoma de Barcelona (UAB), Campus UAB, 08193 Bellaterra, Barcelona, Spain
[b] Research Center for Energy, Environment and Technology, CIEMAT, Madrid, Spain
[c] GAMA Team Department of Applied Physics, University of Barcelona (UB), Barcelona, Spain
[d] PCOT Team, Institute Cartographic and Geological of Catalonia (ICGC), Barcelona, Spain
[e] Department of Chemical, Biological and Environmental Engineering, Universitat Autònoma de Barcelona (UAB), Campus UAB, 08193 Bellaterra, Barcelona, Spain

ARTICLE INFO

Keywords:
Urban land use
Heat waves
Cool roofs
Urban green
WRF BEP+BEM
Urban thermal regulation

ABSTRACT

The frequency and intensity of heat waves (HW) in cities are on the rise due to climate change as well as urban fabric materials and anthropogenic activities that affect heat accumulation. The efficacy of HW mitigation strategies depends on a city's specific and unique morphology, land use, building materials, climate and geography. In this study, we show the effectiveness of cool roofs and vegetation in reducing temperature in the Metropolitan Area of Barcelona (AMB). We use the Weather and Research Forecasting (WRF) model with the urban scheme BEP+BEM, including11 urban classes to simulate a HW that occurred in August 2015. We find that cool roofs reduce temperature best during the day (0.67 °C average and 2.22 °C maximum reductions), while additional green areas moderate temperatures to a lesser degree but also more evenly during the day and at night (average reductions of 0.15 °C and 0.17 °C, respectively). However, when irrigation is increased, the temperature reduction during the day is intensified due to the cooling effect of more evapotranspiration. The thermal regulation of combining the two strategies is the most evenly distributed over the AMB and has the highest impact, with an average and maximum reduction of 1.26 °C and 4.73 °C at 13:00UTC.

1. Introduction

Heat waves (HWs) are extended periods of unusually high atmosphere-related heat stress that usually result in adverse health consequences (Ward et al., 2016) and increased heat-related mortality (Smid et al., 2019; Ingole et al., 2020). The severity and frequency of HWs have increased worldwide in recent decades, and this trend is expected to continue (Kyselý, 2010; Pachauri and Meyer, 2015; Holtanová et al., 2014; Lhotka and Kyselý, 2015). In Europe, a HW in 2003 resulted in more than 70,000 associated deaths (Li and Bou-Zeid, 2013), and the HW of 2010 in Russia and Eastern Europe produced 50,000 fatalities in addition to numerous fires and a

* Corresponding author at: Institute of Environmental Sciences and Technology (ICTA), Building ICTA-ICP, Carrer de les Columnes s/n, Campus of the Autonmous University of Barcelona (UAB), 08193 Bellaterra, Barcelona, Spain.
E-mail address: gara.villalba@uab.cat (G. Villalba).

https://doi.org/10.1016/j.uclim.2021.100863
Received 23 December 2020; Received in revised form 5 March 2021; Accepted 24 April 2021
Available online 6 May 2021

severe drought period (Schneidereit et al., 2012; Barriopedro et al., 2011). During the summer of 2015, many parts of Europe were affected by various extraordinary HWs, most of which had high thermal index values over 35 °C; in addition, western and central Europe experienced tropical nights (Hoy et al., 2017). High temperatures have significant indirect effects, such as increased energy consumption due to the intensified use of air conditioning, which further exacerbates heat accumulation (Tan et al., 2010). For example, during the first week of a HW in Spain in July 2015, electricity increased 8% compared to normal consumption for that time period (REE, 2016).

HW episodes are especially intensified in cities due to urban street canyons, excessive heat accumulation caused by construction materials, a lack of vegetation and green spaces, and/or a lack of open spaces that facilitate the release of waste heat from air conditioning and other energy uses (Stewart and Oke, 2012). This microclimatic effect can be intensified during hot summers, and exposure to high temperatures can lead to heat stress (Guarino et al., 2014). Extremely high temperatures can increase the demand for energy and water usage and lead to an increase in harmful air pollutants (Santamouris, 2014). The urban heat island effect (UHI) refers to the phenomenon in which urban areas have higher temperatures than their surrounding rural and peri-urban areas (Oke, 1982; Moreno-garcia, 1994; Arnfield, 2003). That is why, in urban regions, HWs are often further intensified by the UHI effect.

Currently, the urban landscape is home to more than half of the world's population, and projections indicate that by 2050, it will rise to 70%, reaching 6.3 billion inhabitants (UN, 2015). In Europe, 75% of the population currently resides in cities, and this number is expected to grow to 82% by 2050 (Guerreiro et al., 2018; Habitat, 2013). The growing urbanization accompanied by an aging population trend is intensifying the impact of heat waves, and there is an urgent need to implement mitigation measures to reduce heat stress (Luber and McGeehin, 2008). In recent decades, different strategies have been proposed and developed to reduce the negative effects of urban heat during HWs in urban areas, such as the use of reflective materials on roofs to increase albedo. These “cool” roofs increase the reflection of incident solar radiation and reduce total net radiation (Gago et al., 2013; Li et al., 2014) as well as heat accumulation in buildings (Akbari et al., 2001; Campra et al., 2008; Synnefa et al., 2008; Campra, 2011; Yang et al., 2015; Li and Norford, 2016; González et al., 2019). A cool roof is characterized by high solar reflectance and an albedo value above 0.65, according to the Environmental Protection Agency (EPA) of the United States, and high infrared emission, thereby reducing surface temperature (Bretz and Akbari, 1997) since cooler surfaces have lower heat convection (Synnefa and Santamouris, 2012). This simple strategy is especially attractive because it promotes existing unused rooftops worldwide, estimated to be 20% of the total area in cities (Akbari et al., 2009).

A similar strategy is the implementation of green roofs, in which roofs are partially or completely covered with vegetation. This strategy not only reduces temperature through evapotranspiration (Qiu et al., 2013) and changes albedo but also contributes to reductions in air pollutants (through deposition) and carbon dioxide (through photosynthesis) (Getter and Rowe, 2006; Rowe and Getter, 2015; Li et al., 2010). The effect of urban green spaces on decreasing temperatures has been studied (Fallmann et al., 2013; Feyisa et al., 2014; Demuzere et al., 2014; Yu et al., 2018) for different types of vegetation, park sizes and city climates (Gago et al., 2013; Bowler et al., 2010). Some studies have verified that in green areas, there is a decrease in temperature within a one-kilometer radius (Upmanis et al., 1998), with green spaces being up to 4 °C cooler than their surroundings (Eliasson, 1996). Other studies aimed to analyze HW mitigation strategies at the building or neighborhood scale (Jaffal et al., 2012; Zinzi and Agnoli, 2012; Morini et al., 2018), but the results of these studies cannot be extrapolated to determine the effects for the entire city due to the city's land-use complexity, geography, and climate (Cadenasso et al., 2007; Li et al., 2014; Geletič et al., 2016).

Limited modeling efforts have been undertaken to determine the effects of HW mitigation strategies in entire metropolitan areas because it is difficult to work at such fine resolutions and correctly represent such varied land-use heterogeneity. As pointed out by a review of reflective and green roof mitigation technologies in urban environments (Santamouris, 2014), most of the existing studies are based on mesoscale simulations using regional models that often do not fully represent the heterogeneity of urban land use or the complex physics occurring in urban canopies. For example, Millstein and Menon (2011) use a regional model to study the large-scale effect of increasing albedo of US cities up to an additional 0.115 and conclude that cool roofs and pavements contribute to decreasing average afternoon summertime temperatures by 0.11–0.53 °C. Although this study provides an understanding of the large-scale effect of these strategies, the simplified urban parameterization does not adequately account for the surface heterogeneity at the urban scale, significantly simplifying the role of urban heterogeneity in the efficiency of cooling strategies at the city level. Similarly, Oleson et al. (2010) studied the effects of white roofs on urban temperature using a global climate model and found that by incrementing the albedo to 0.9 in all urban areas, the annual mean heat island effect decreased by 33%. However, because of the coarse spatial resolution of these simulations (1.9° latitude by 2.5° longitude), changes in surface climate caused by the increase in roof albedo are not well understood.

Other studies have coupled regional models with urban canopy models to more accurately represent the surface heterogeneity in urban environments (Brousse et al., 2016; Ribeiro et al., 2021; Zonato et al., 2020). Li et al. (2014) determined the significant cooling effect of green and white roofing strategies over the Baltimore-Washington metropolitan area during a heat wave period using the Weather Research and Forecasting (WRF) model in conjunction with the Princeton Urban Canopy Model (PUCM). The PUCM satisfactorily resolves the effects of surface heterogeneity in urban canyons, but the urban parameterization is limited to three urban land class typologies (low-density residential, high-density residential, and industrial/commercial), which might not adequately describe the heterogeneity of cities. Similarly, simulations incrementing the green areas of Melbourne from 27% to 40% have shown a reduction in nighttime temperatures of 1.5 °C (Jacobs et al., 2018). In the city of Athens, Papangelis et al. (2012) found that when the vegetation fraction was increased from 27% to 50%, nighttime temperatures were reduced by 1.98 °C, albeit no cooling effect was found during the daytime. Both of these simulations were resolved at the urban scale, with resolutions between 500 and 2000 m, but generally simplified the urban fabric by defining only a few urban built environment typologies. High-resolution simulations that account for urban morphology and its complex heterogeneous land use, including the interactions between the local climate (i.e., solar radiation

intensity, ambient temperature and humidity, and wind speed) and the built environment (i.e., thermal capacity and optical variables) are needed to guide policies for sustainable urban planning and design.

In this study, we aim to add to this pool of knowledge and advance our understanding of the interactions between land/roof use and the urban atmosphere as well as the specific morphology, climate, and geography of cities and determine the city-wide effects of several strategies for mitigating the negative effects of heat during HWs. We use a meteorological model (WRF) coupled with an urban canopy model (UCM), building effect parameterization (BEP) and a building energy model (BEM) (Martilli, 2002; Salamanca and Martilli, 2010; Salamanca et al., 2010; Brousse et al., 2016; Ribeiro et al., 2021). In recent years, modeling efforts have concentrated on enhancing resolution by improving urban canopy parameters (UCPs) (Zonato et al., 2020). Several studies show that a good representation of UCPs allows accurate simulation of the temperature variability in urban areas (Salamanca et al., 2012; De Ridder et al., 2015; Li et al., 2018). BEP captures urban surfaces in three dimensions and considers buildings as sinks and sources of heat and as momentum and turbulent energy, while BEM parameterizes the anthropogenic heat released from inside buildings to the outer atmosphere along with the thermal building energy consumption.

The Metropolitan Area of Barcelona (AMB) serves as a case study, and the mitigation strategies analyzed are based on future green infrastructures defined by the Metropolitan Urban Master Plan (PDU, 2019. We are able to characterize the urban fabric in great detail thanks to the high-resolution urban fraction data available from the cartography of urban land uses and the classification of the local climate zones (LCZs) into 11 urban classes (Stewart and Oke, 2012; Gilabert et al., 2021) at a 100-m resolution. The model is used to simulate the heatwave that affected the AMB and much of Europe during most of July 2015, when the presence of an anticyclonic ridge from the Azores along with an inrush of very warm air from northern Sahara caused the daily average temperature to exceed 33.1 °C for more than three consecutive days. Three mitigation scenarios are explored and compared to the reference scenario to quantify the potential reductions resulting from the various land-use changes: 1) implementing cool roofs, 2) increasing the vegetation fraction, and 3) a combination of strategies 1 and 2.

This article is organized as follows: Section 2 briefly presents the study area and the heat wave period chosen for the case study; Section 3 is dedicated to the methods used, including the WRF BEP + BEM configuration and validation methods; section 4 provides a description of the heat wave mitigation scenarios; Section 5 is dedicated to the validation of the model set up with the heat wave reference scenario; Section 6 summarizes the main results for each mitigation strategy; Section 7 discusses the results in light of heterogeneous urban land use and how the various mitigation strategies affect the energy balance; and finally, Section 8 provides the conclusions.

2. Case study area and period of interest

The Metropolitan Area of Barcelona (AMB) is located in the northeast if the Iberian Peninsula in the Euro-Mediterranean region (Fig. 1a), The AMB's coast line is oriented from southwest to northeast, a littoral range (near 500 m altitude) in the northwest and two rivers in the northeast and the southwest. Its Mediterranean climate is characterized by dry summers, with a regime of breezy conditions and warm temperatures (25–27 °C) influenced by the thermoregulatory effect of the sea, which in turn intensifies the heat sensation due to the increase in humidity. The day and night transitions of the sea/inland breeze together with the UHI effect cause a complex structure in the atmospheric boundary layer, modifying the temperature and dispersion of contaminants (Soler et al., 2011). Anticyclonic situations that involve intense heat waves associated with severe pollution episodes are common during the summer. The AMB has been identified as an urban area with high vulnerability due to the effects of climate change (Giorgi, 2006) and is expected to experience an increasing frequency of longer lasting and more severe heat waves (Ballester et al., 2009; Altava et al., 2015). This region covers an area of 636 km^2 and has a population of more than 3,000,000 inhabitants (the 6th largest urban area in Europe), with

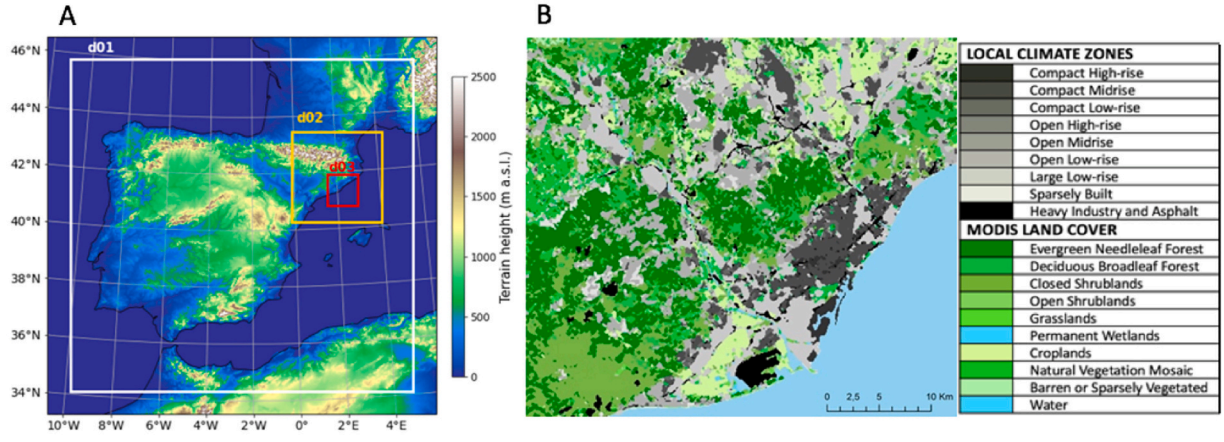

Fig. 1. Panel (a) shows the three nested domains used to run the WRF BEP + BEM, where the innermost domain is 121 km by 121 km, centered around the Metropolitan Area of Barcelona at a 1 km resolution, shown in more detail in panel (b) which shows the various land-use categories: 11 urban Local Climate Zone categories and MODIS Land Cover categories for the rest.

Table 1
Summary of parameters characterizing each scenario.

	Built types	Definition	% of AMB area	Total roof space over total building (%)	Reference scenario	Cool roof scenario	Greening scenario	Combined scenario
					Albedo			
 LCZ 1	Compact high-rise	Tall buildings, few or not trees. Concrete, steel, Stone and glass materials	0.41	46.17	0.15	0.85	0.15	0.85
 LCZ 2	Compact midrise	Dense mix of midrise buildings. Few or not trees. Mostly paved: Stone, brick tile and concrete materials	7.36	48.30	0.15	0.85	0.15	0.85
 LCZ 3	Compact low-rise	Dense mix of low-rise buildings. Few or not trees. Mostly paved: Stone, brick tile and concrete materials.	1.60	39.43	0.15	0.15	0.15	0.15
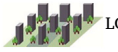 LCZ 4	Open high-rise	Open arrangement of tall buildings to tens of stories. Abundance of pervious land cover. Concrete, steel, Stone and glass materials	0.02	4.34	0.14	0.85	0.14	0.85
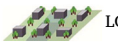 LCZ 5	Open midrise	Open arrangement of midrise buildings. Abundance of pervious land cover. Concrete, steel, stone, and glass construction materials.	0.68	15.12	0.15	0.85	0.15	0.85
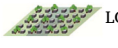 LCZ 6	Open low-rise	Open arrangement of low-rise buildings. Abundance pervious land cover (low plants, scattered trees).Wood, brick, stone, tile, and concrete construction materials.	8.33	11.88	0.14	0.14	0.14	0.14
 LCZ 8	Large low-rise	Open arrangement of large low-rise buildings. Few or no trees. Land cover mostly paved. Steel, concrete, metal, and stone construction materials.	11.96	30.35	0.16	0.85	0.16	0.85
 LCZ 9	Sparsely built	Sparse arrangement of small or medium-sized buildings in a natural setting. Abundance of pervious land cover.	2.24	2.20	0.13	0.13	0.13	0.13
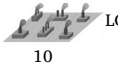 LCZ 10	Heavy industry	Low-rise and midrise industrial structures (towers, tanks, stacks). Few or no trees. Land cover mostly paved or hard-packed. Metal, steel, and concrete construction materials.	0.71	10.75	0.16	0.16	0.16	0.16
 LCZ E	Asphalt	Featureless landscape of rock or paved cover. Few or no trees or plants. Zone function is natural desert (rock) or urban transportation.	2.61	6.80	0.16	0.16	0.16	0.16
Total area of urban LCZ	519 km^2		35.92					
Total non-urban area	925 km^2		64.08		0.14	0.14	0.14	0.14
Total area of AMB	1444 km^2		100					

population densities higher than those of New York or Tokyo, reaching 160 inhabitants/ha in the city center.

For our study region, we use the heat wave (HW) definition from the Meteorological Service of Catalonia (SMC), which describes a HW as an event in which the maximum daily temperature exceeds the 98th percentile of the summer temperatures for at least three consecutive days (SMC, 2015). The HW selected as a case study took place between 29/06/2015 and 07/07/2015; during this time, the daytime temperatures reached 40 °C in the interior of the AMB and 35 °C in the coastal area, and the nighttime temperatures did not go below 25 °C in some downtown neighborhoods for five consecutive days. For a more detailed description of the HW and atmospheric conditions, please see Supplementary Information Section 2.

3. Methods

We used the Weather Research and Forecasting (WRF) model version 4.0 (Skamarock et al., 2019) coupled with the urban canopy model (BEP + BEM) (Salamanca et al., 2010). The WRF is a numerical weather prediction (NWP) system used for regional forecasting and atmospheric research that solves the non-hydrostatic, compressible Euler equations using terrain-following vertical coordinates (Skamarock et al., 2019). The BEP + BEM scheme (Salamanca and Martilli, 2010) is currently the most sophisticated urban scheme; it is based on the coupling of a multilayer canopy model (BEP), which recognizes the three-dimensional nature of urban surfaces and the fact that buildings vertically distribute sources and sinks of heat, moisture, and momentum through the whole urban canopy layer, and a building energy model (BEM), which explicitly resolves exchanges of energy between the interior of the buildings and the outdoor atmosphere. The WRF BEP + BEM combination has been previously evaluated and used to simulate urban meteorology, showing good agreement with observed data with various urban parametrizations and for different urban regions (Salamanca et al., 2011, 2012; Sharma et al., 2014; Ribeiro et al., 2021). The WRF configuration consists of three two-way nested domains with horizontal resolutions of 9 km (150 × 145; covering the entire Iberian Peninsula and northern Africa; domain 1), 3 km (118 × 118; covering the entire Catalan territory and extending to the north above the eastern Pyrenees; domain 2), and 1 km (121 × 121; covering the AMB; domain 3), as shown in panel (a) of Fig. 1. The model is implemented with 57 pressure-based vertical layers, ranging from the surface to the top at 50 hPa; the resolution in the lowest 50 m is constant (at approximately 5 m) and a progressively increasing resolution is applied above this height, resulting in 36 numerical layers in the lowest 1.5 km. This allows for a better representation of the vertical fluxes within the urban boundary layer (UBL).

The initial and boundary conditions were taken from European Centre for Medium-Range Weather Forecasts (ECMWF) ERA5 model-based reanalysis datasets (C3S, 2017), with a 31 km horizontal resolution and a 6-h separation for the lateral boundary conditions. Additionally, sea surface temperature is updated daily with ERA5 data (Hersbach et al., 2020). The physical options for the simulations in this study include (1) the WRF single-moment 6-class scheme (Hong and Lim, 2006) for microphysics, (2) the Rapid Radiation Transfer Model for General Circulation Models (RRTMG) scheme (Iacono et al., 2008) for shortwave and longwave radiation, (3) the Kain-Fritsch scheme (Kain and Kain, 2004) (only for the outermost domain) for cumulus parameterization, (4) the 4-layer Noah land surface model (LSM) (Chen and Dudhia, 2001) for nonurban surfaces, and (5) the Bougeault-Lacarrère (PBL) scheme (Bougeault and Lacarrere, 1989) and Monin-Obukhov similarity scheme with Zilitinkevich thermal roughness length for the surface layer.

For the land-use/land-cover (LCLU) classification, the WRF model is adapted and applied to domain 3 following the indications by Martilli et al. (2016). The local climate zones (LCZs) model developed by the World Urban Database and Access Portal Tools (WUDAPT) initiative (Bechtel et al., 2015; Brousse et al., 2016) was used and improved through the reclassification and integration of high-resolution LCLU maps, such as the Urban Atlas 2012 (https://land.copernicus.eu/local/urban-atlas) and the LCLU AMB 2015 (Gilabert et al., 2021). The LCZ model establishes a framework for classifying eleven different urban areas with distinct urban cover,

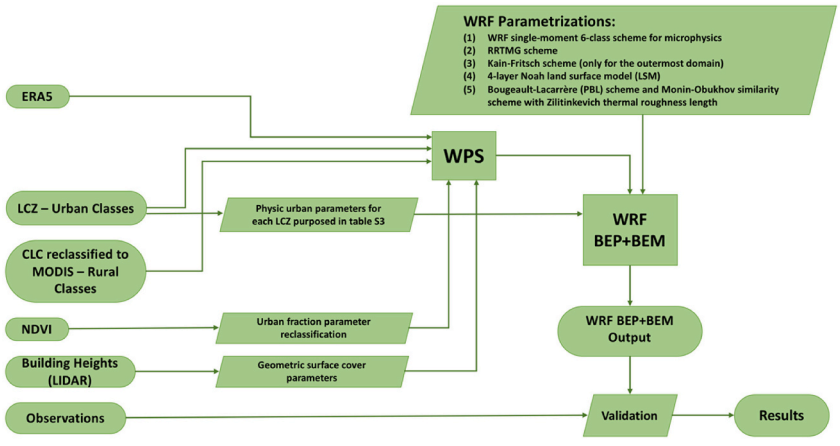

Fig. 2. A flowchart depicting the roadmap of the study as well as the interactions between different physical parameterizations in the modeling process.

population density, structure, material, and human activity, as shown in Table 1 (Stewart and Oke, 2012). The AMB is made up mostly of LCZs 2 (compact midrise), 6 (open low rise), and 8 (large low rise). Altogether, the eleven urban LCZs cover close to 36% of the entire AMB (as shown in Fig. 1(b) in tones of gray). The classification of the rest of domain 3 was completed with the 44 Corine land cover classes for 2018, reclassified with MODIS data (shown in Fig. 1(b) in shades of green).

Specific values of multiple urban parameters defining the average thermal and radiative properties (albedo and emissivity) of the buildings as well as the energy consumption and efficiency of air conditioning units (i.e., thermal power) are assigned to each LCZ and used in the BEP + BEM scheme. The albedo of the roofs and the ground was calculated for each LCZ according to Liang (2001) and based on 12 monthly images from Landsat 5 TM with a 30 m resolution (USGS, 2019) and ranges from 0.13 to 0.16, as shown in Table 1. The roof and ground emissivity values are calculated based on the normalized difference vegetation index (NDVI) using Landsat 8 OLI/TIRS images (Vermote et al., 2016), according to the method proposed by Ndossi and Avdan, 2016. A thermal efficiency default value of 0.75 was used for all the LCZs. In each LCZ, the heat released by AC units is calculated as the amount emitted when indoor temperatures are maintained at 21.5 °C, with a comfort range of ±3.5 °C. All the thermal and radiative parameters for each LCZ are summarized in Supporting Information S3. These parameters were determined through communications with urban planners and architects of the AMB as well as remote sensing and some values proposed by Ribeiro et al. (2021) for the AMB.

The BEP + BEM also requires geometric and surface cover parameters, such as building height and width, street width, and built and vegetation fractions, which are not defined for each LCZ but are directly introduced into the grid cells of the innermost domain, as described by Pappaccogli et al. (2017). Building and wall height data were gathered from LiDAR data and a digital surface model with a resolution of 2 m, freely available at the Institute Cartographic and Geological of Catalonia (ICGC, 2019). Once the building height map was generated, the Urban Multiscale Environmental Predictor (Lindberg et al., 2018) was applied to generate the wall heights, and a histogram of building heights was generated as proposed by Pappaccogli et al. (2017).

The urban fraction is calculated using NDVI data from Landsat 8 OLI/TIRS images with a 30 m resolution (USGS, 2019). These images were reclassified based on ICGC categories (Alamús et al., 2018), where NDVI <0 represents water or artificial cover, $0 <$ NDVI <0.2 represents bare soil and dead vegetation, and $0.2 <$ NDVI represents all vegetation. The NDVI has been shown to be a good indicator for differentiating urban areas from vegetated areas, especially at our latitudes and in metropolitan areas (Yuan and Bauer, 2007). With that information, it is possible to generate an urban fraction map of impermeable surfaces where NDVI is less than 0.2. The rest of the area is considered urban vegetation, of which 30% is treated as permeable bare soil by the Noah LSM. These three fractions (urban, vegetation, and bare soil) add up to 1, as shown in Table 1. The simulation setup described in the previous paragraphs is summarized in Fig. 2.

The simulations cover 12 days of the study period, starting on 24/06/2015 and ending on 07/07/2015, discarding the initial days from 24/06/2015 to 03/07/2015 as spin-up days and focusing on the three hottest days (04/07/2015–06/07/2015). The reference case was validated using hourly observations of temperature, relative humidity, wind speed and direction provided by the 13 meteorological stations inside the AMB and three rural stations from the Meteorological Service of Catalonia (see Supplementary Material Fig. S1 and table S1).

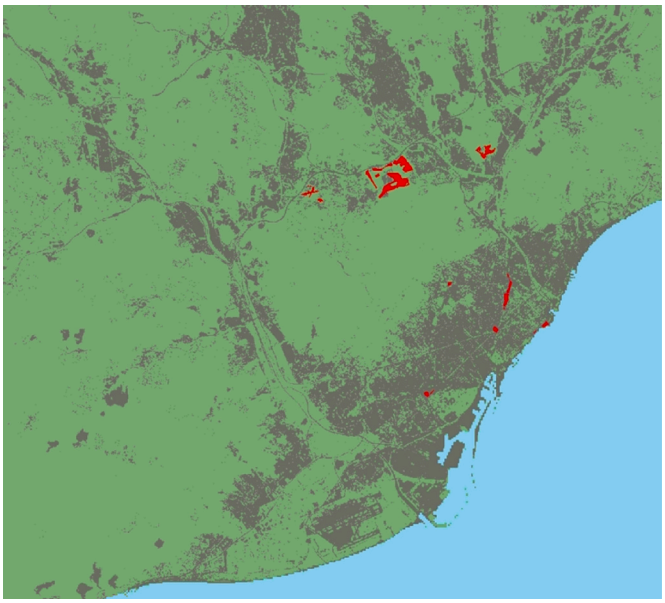

Fig. 3. Urban fraction (gray) and vegetation fraction (green) based on NDVI reclassification. The additional 255.64 ha of urban green proposed by the Urban Master Plan are shown in red. (For interpretation of the references to colour in this figure legend, the reader is referred to the web version of this article.)

4. Mitigation scenarios

The next three sections describe the HW mitigation scenarios, summarized in Table 1.

4.1. Scenario 1: increasing cool roofs

The "cool roof" scenario entails incrementing the albedo of certain rooftops to 0.85 by painting them white. This albedo value is well over the 0.65 threshold for cold roofs (Li et al., 2014) and has been examined by other authors as well such as Sharma et al. (2016). The albedo is implemented for the rooftops in LCZ's 1, 2, 4, 5, and 8, as shown in Table 1. The buildings in these LCZs have mostly accessible flat roofs, which are easier to paint than the duo-pitch roofs found in LCZs 6 and 3, the albedo of which remains at 0.14 and 0.15, respectively.

4.2. Scenario 2: greening

This mitigation scenario consists of increasing urban green areas according to the targets set by the Urban Master Plan (PDU) of the AMB (https:\\urbanisme.amb.cat\en\home), which calls for the addition of 6 urban parks and green areas with a total of 255.64 ha by 2030, as shown in Fig. 3. A new NDVI map is generated with the new additional green areas, and consequently, a new green fraction and urban fraction is determined for each grid cell in the innermost domain (1 km × 1 km), assuming that the urban morphology (buildings and street width) remained the same. When we sum the fractions of the urban grid cells in the AMB in this scenario, the vegetation fraction increases from 32.54 to 35.92 and the urban fraction decreases from 53.04 to 48.68, as shown in Table 1.

The reference case considers a daily irrigation of 2 L/m^2 from 4:00 to 5:00 UTC, as reported by Ajuntament de Barcelona (2013). For the greening scenario, we ran two simulations to explore the effects of irrigation of urban green areas on the temperature of the AMB by increasing irrigation from 2 to 5 L/m^2·day, a value above current practices but still within the recommended limits established by the same report.

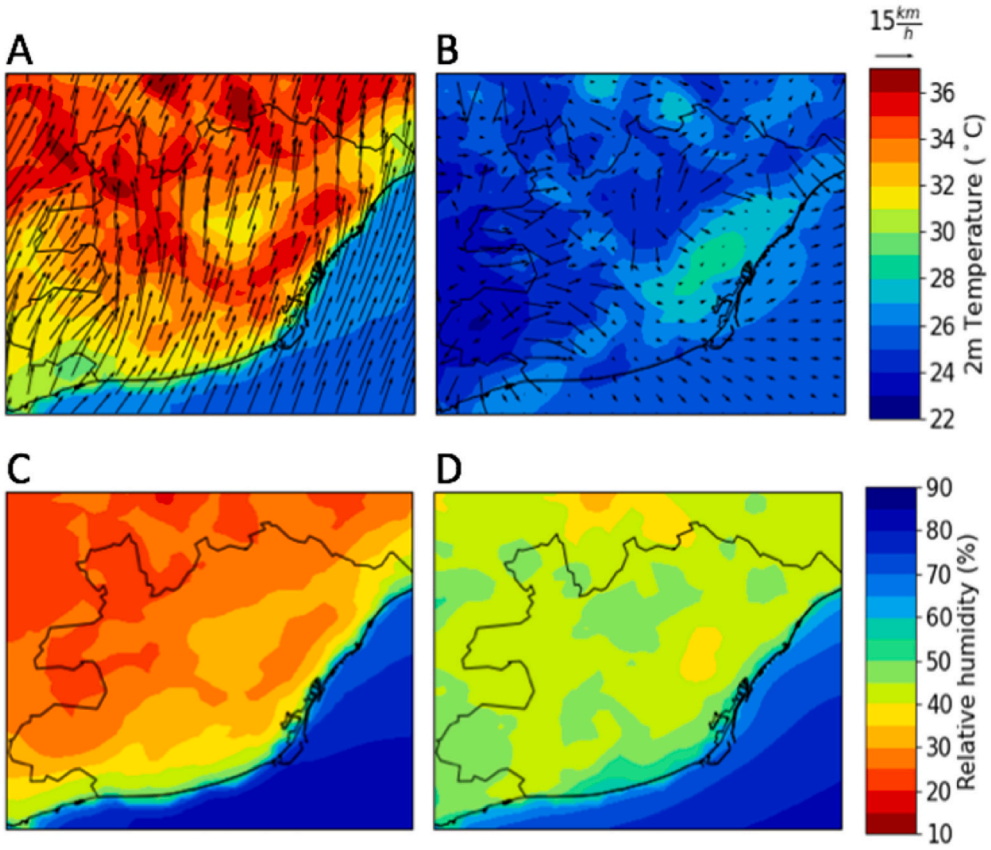

Fig. 4. Reference case averages of three days during the heat wave: a) Temperature 2 m (with wind direction) daytime, b) Temperature 2 m (with wind direction) nighttime, c) RH daytime, d) RH nighttime.

4.3. Scenario 3: combined scenario

The last scenario is a combination of the cool roofs and the additional urban green space, with a higher irrigation (5 L/m^2·day instead of 2 L/m^2 ·day). The aim of simulating this scenario is to see to what extent these two mitigation strategies can complement each other to obtain more prolonged and/or even distribution of thermal regulation.

5. Validation of reference scenario

The simulation of the heat wave episode (4/06/2015 to 6/06/2015) is validated in terms of temperature and relative humidity by comparison with observation data available from 16 weather stations (supplementary material Fig. S1, table S1). The root mean square error (RMSE), mean bias (MB) and Pearson's correlation (R) are calculated over the entire simulation, distinguishing between day and night, LCZ, and type of weather station (urban or rural).

A strong positive correlation (0.9 for temperature and 0.8 for relative humidity) is found between the observations and the model (see Fig. S4 in the Supplementary Information). In terms of the temperature, we do not observe a significant difference in the RMSE or R for the daytime and nighttime urban/rural areas, with 1.5 °C for the RMSE and 0.9 for the R. However, a negative BIAS (−0.3 °C) is seen during the day, in contrast with the positive BIAS (0.6–0.9 °C) observed during the night, resulting in a positive bias (0.3 °C) for the whole day. The positive BIAS during the night could be related to a limitation in the definition of soil moisture, which is one of the

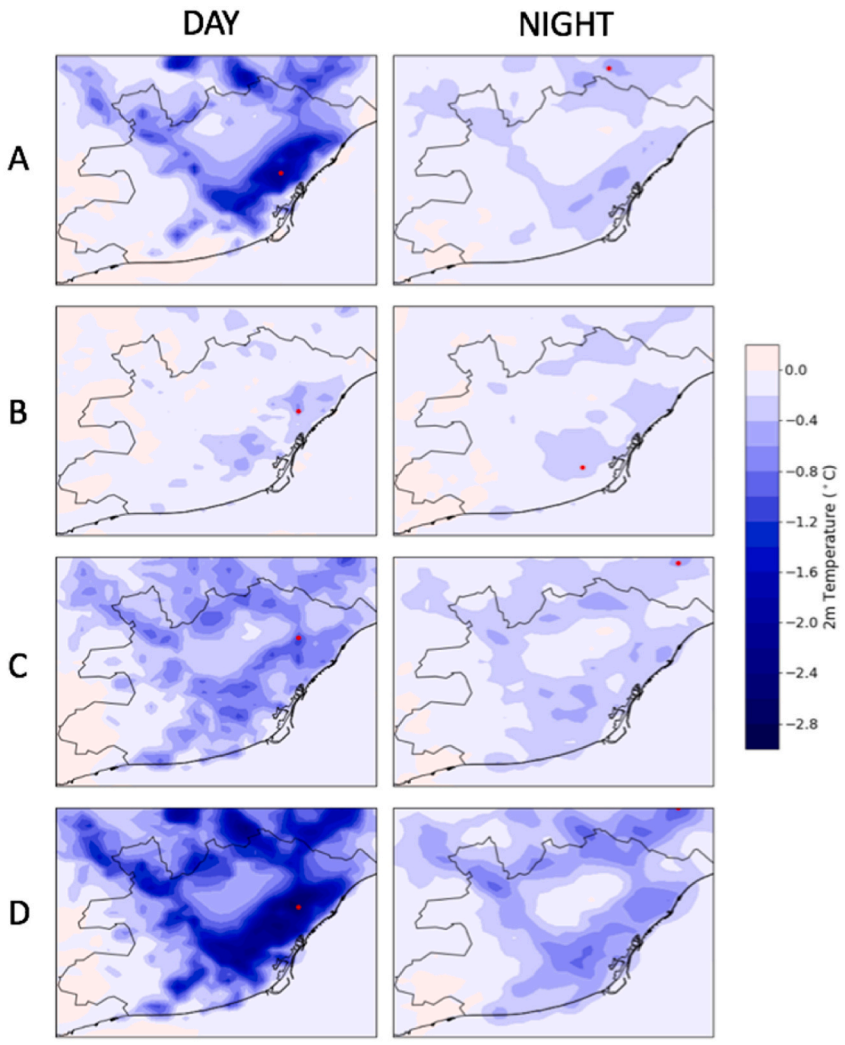

Fig. 5. The 2 m temperature difference between the reference case and the scenarios: a) Cool roof, b) Greening with standard irrigation 2 L/m^{2}day c) Greening with increased irrigation to 5 L/m^{2}day and d) Combined. The 2 m temperature is the average temperature over the daytime (9:00–15:00 UTC / 11:00–17:00 local time) and nighttime (19:00–5:00 UTC / 21:00–7:00 local time) for the three hottest days of the simulation: 4/06/2015 to 6/06/2015. The red dots represent the point with the highest temperature reduction. (For interpretation of the references to colour in this figure legend, the reader is referred to the web version of this article.)

most difficult variables to capture (Chen et al., 2007). In general, the model exhibits a better performance over the rural stations, especially during the nighttime, than over the urban stations, which cover more heterogeneous terrain and are thus more difficult to simulate, as has been found by other authors (Jacobs et al., 2018; Ribeiro et al., 2021). On the other hand, in terms of the relative humidity, the model presents errors that range between 8 and 16% on average for all the days, with the highest errors (21%) recorded during the nighttime. A negative bias is seen throughout the whole day (−4%), especially during the night, when it reaches −9% for the rural stations. Relative humidity biases may be related to biases found, for example, in temperature but have lower values because surface patterns and day/night cycles do not resolve as well as temperatures (Ribeiro et al., 2021; Jiménez-Esteve et al., 2018; Jandaghian et al., 2018).

Overall, there is congruence between the observed behavior and the simulated HW used in the case study. Fig. 4 shows the daytime and nighttime modeled temperatures for the three hottest days (4/06/2015 to 6/06/2015). As was observed during the actual HW, the model shows that maximum temperatures exceed 35 °C during the day in the urban zones located in the most continental part of the AMB, where the sea has less thermoregulatory influence. The coastal and more peri-urban areas were on average 4 °C lower. During the day, the lowest simulated temperatures are found at locations with more abundant vegetation or in areas with higher altitudes, where the vertical gradient has an influence; these temperatures oscillate between 28 °C and 30 °C and coincide with those reported by the weather report (Meteorological Service of Catalonia SMC, 2015). The nighttime simulations show that the lowest temperature is approximately 23 °C, similar to data from most weather stations within Barcelona.

In terms of convection, the model simulates well the characteristic low wind speeds associated to heat waves. The daytime breezes (of 12.7 km/h or 3.5 m/s) which typically start at 9:00 and end at 16:00 (local time) were well depicted by the simulations, as well as the nighttime land-sea breezes, which were generally calmer (4.9 km/h or 1.4 m/s), lasting from 23:00 to 5:00 (local time). The RMSE and MB ranged between 0.94 and 2.0 and − 1.8 to 0.9 m/s, respectively, depending on the location of the meteorological station. Overall, the winds ranged between 0 and 3 out of 12 in the Beaufort scale (Huler, 2004) and were deemed rather insignificant during the HW, as has been previously seen by other authors (Ackerman and Knox, 2012). Wind direction also showed acceptable validation, with a MB ranging between −20° a 24° during the day when breezes were highest. Furthermore, we expect wind direction to have little influence over the AMB over the study period given the low wind speeds.

The relative humidity level during the day is between 30 and 40%, which indicates that the heat index (an index that combines air temperature and relative humidity) was 1–2 °C above the dry air temperature (Rothfusz and Headquarters, 1990). At night, the relative humidity increases by an order of 10%, but the temperature is low, which translates into a heat index equal to the temperature of dry air. Overall, the good performance of our model lends confidence to simulations of heat mitigation strategies.

6. Results

The results are analyzed during the day, when the heat stress and energy consumption are the highest, that is, from 9:00 to 15:00 UTC (11:00 to 17:00 local time), and at night, from 19:00 to 5:00 UTC (21:00 to 7:00 local time), when there is no shortwave radiation and irrigation takes place. In the next few sections, we highlight the most significant results for each scenario in terms of these two time periods over the five-day simulations.

6.1. Cool roofs

In the cool roof scenario, net radiation is greatly reduced during the day due to the increased reflective capability of all the new white roofs, significantly cooling the AMB during the daytime. Fig. 5a (day) shows the reductions in daytime modeled temperature averaged over a 7-h period (09:00 to 15:00 UTC). The highest reduction (2 °C) is seen in the northern region of Barcelona, close to the coast, with the most compact, densely populated areas and highest total roof area. At the southern end of the city, which is characterized by peri-urban agriculture, sparse construction, and industrial areas, the cooling effect of white roofs is not as significant, and temperature reductions range between 0 and 0.4 °C. Furthermore, sea breezes, which normally occur at midday, spread the cooling effect of white roofs through advection to inland rural areas and nonmodified urban areas. At night, the temperature reductions are less significant because there is no shortwave radiation, and the change in albedo does not have as much of an effect, as can be appreciated in Fig. 5a (nighttime). However, a decrease in temperature is still noticeable (up to 0.6 °C), because lower temperatures during the day result in less heat being stored and released during the night (Li et al., 2014). The simulation results show maximum temperature reductions of 3.83 °C and 1.63 °C at 13:00 UTC (15:00 local time) and 5:00 UTC (7:00 local time), respectively (table S4). The locations where this occurs are represented by red dots in Fig. 5a (day and night). These temperature reductions are comparable to other studies that simulate increase in albedo as a thermal regulation strategy, such as 2 °C reduction estimated for the city of Terni, Italy (Morini et al., 2016), and potential 2.5 °C reduction for the Baltimore-Washington metropolitan area (Li et al., 2014).

The modeled relative humidity shows an increase during the day (1.6% on average), which we attribute to the decrease in temperatures due to lower sensible heat fluxes from the rooftops. Consequently, as sensible heat decreases, so does the boundary layer height, as shown in Fig. 7, after 12:00 UTC, thereby reducing the air mixture and increasing the relative humidity. See Fig. S5 of the supplementary material for a summary of the results for relative humidity.

6.2. Greening scenario with various irrigation schemes

The simulations show that increasing urban green areas by an additional 255.64 ha, as proposed by the Urban Master Plan, reduces the thermal storage capacity of the city's surface, and consequently reduces the temperature reduced, albeit not as significantly as in

the cool roof scenario. As we can see in Fig. 5b, the thermal regulation provided by the increment of green space is more or less similar during the day and night, with average (over a given time period and for all the urban areas) temperature reductions of up to 0.15 °C during the day and 0.17 °C at night in similar urban areas of the AMB. The maximum temperature reductions are 1.70 °C and 1.24 °C, achieved at 11:00 UTC and 3:00 UTC, respectively. The difference between the daytime and nighttime impact is accentuated when we increase irrigation from 2 L to 5 L/m^2 day. Then, temperatures are reduced further during the day, because the evapotranspiration process is intensified, thereby incrementing latent heat to the detriment of sensible heat, as shown in Fig. 5c. We estimated maximum temperature reductions of 2.46 °C and 1.44 °C at 15:00 and 1:00 UTC, respectively (Supporting Information table S4). The average daytime temperatures also decreased considerably, from 0.15 °C with 2 L/m^2 day to 0.61 °C with 5 L/m^2 day. With increased irrigation, the most notable temperature reduction occurs during the day, because the evapotranspiration process occurs when there is incident shortwave radiation. Even though urban green areas have increased in very specific areas, as shown in Fig. 3, and not in the more evenly distributed way of cool roofs, cooler air from green areas diffuses over the AMB due to the advection of sea breezes during the day, as shown in Fig. 5c on the left. The relative humidity also increases more during the day (by an average of 2.2% across the entire region of interest). Note that the boundary layer also decreases with respect to the reference case (Fig. 7).

6.3. Combined scenario

This last scenario has the combined effect of reducing temperatures during the nighttime due to more urban green areas and during the daytime due to increased albedo and irrigation (see Fig. 5d), thereby abating the heat wave effect throughout a 24-h period. Furthermore, white roofs lower the temperature in the central and dense urban areas, whereas more green roofs and irrigation help lower the temperature in the peripheral areas. The daytime temperature reductions in this scenario are the most widespread over the AMB and the most significant of all the scenarios, reaching an average temperature reduction of 1.26 °C over 49% of the urban surface

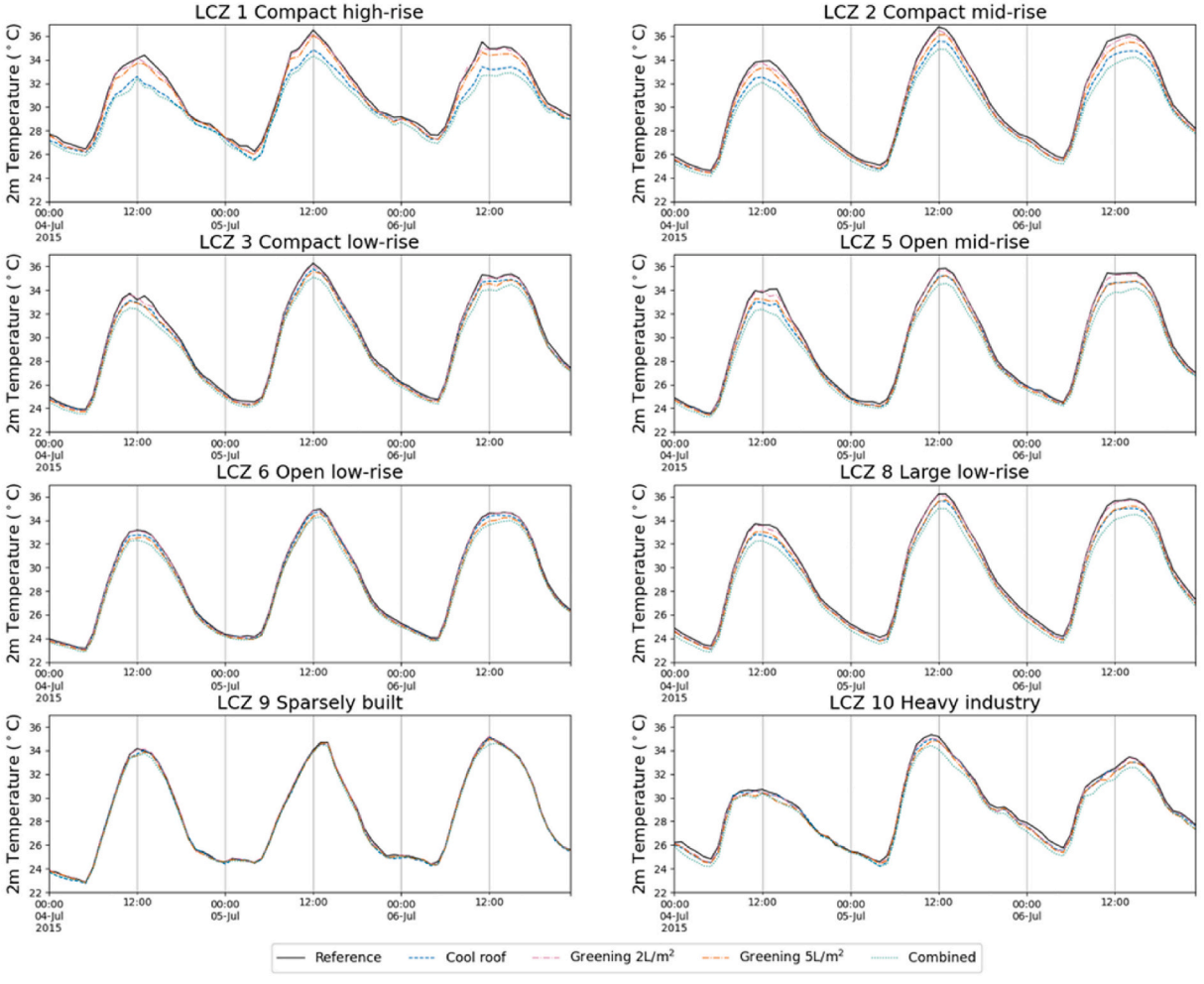

Fig. 6. 2 m temperature profile of various LCZ's for the three scenarios: Cool roof, greening and combined during the three hottest days of the simulation: 4/06/2015 to 6/06/2015.

areas of the AMB, whereas a reduction of only 15% was achieved in the cool roof scenario. The nighttime simulation shows a similar diffusive effect, reaching average temperature reductions of 0.49 °C, higher than any previous scenario. The simulations show maximum reductions of 1.88 °C and 4.73 °C at 19:00 UTC (21:00 local time) and at 13:00 UTC (15:00 local time), respectively (table S4).

The combined scenario has the most notable increase in near-surface relative humidity (up to 3.5%) which is explained by the fact that it achieves 1) the most significant temperature reductions, 2) the lowest mixing height (see Fig. 7), and 3) an enhanced evapotranspiration process (either directly from the soil or from transpiration from plants).

7. Discussion

7.1. The role of urban heterogeneity on temperature reduction potential

The implementation of cool roofs on residential and industrial buildings causes a heterogeneous reduction in temperature, since there is variability both temporally (albedo affects daytime temperatures) and spatially (the implementation of white roofs depends on building typologies). This is especially significant for the AMB, which has highly heterogeneous land use, as shown in Fig. 1b. The impact of incrementing urban green space also depends on urban morphology and its effect on convection. We thus find it informative to show the temperature reduction potential of the scenarios tested for each LCZ (Fig. 6), which vary in building density, morphology, and total roof surface area, as described in Table 1. The greening scenarios with both irrigation schemes resulted in similar behaviors in all the LCZs (with temperature reductions between 0.1 and 0.8 °C), lowering the maximum daytime temperatures from 34.04 to 33.44 °C. This reflects the diffusive nature of the cooling effect of incrementing green space, regardless of the urban morphology. In contrast, the increment in albedo led to more pronounced differences in temperature reductions among the LCZs. The white rooftops have the greatest cooling effect for LCZ1 (compact high rise), decreasing temperatures by up to 2.5 °C at noon during the hottest days of the HW. However, less than 1% of the AMB has this type of urban LCZ, and consequently, such high cooling effects are not widespread throughout the city. Furthermore, it is difficult to conclude how much of the temperature reduction is due to the net radiation of LCZ1 and how much is because LCZ1 is surrounded by LCZ2 (compact midrise) in the AMB.

The AMB is made up mostly of LCZ2, LCZ6 (open low rise), and LCZ8 (large low rise), which account for 20, 23, and 33% of the urban area, respectively, as shown in Table 1. The white roofs on the compact mid-rise buildings belonging to LCZ2 lower temperatures by 1.2 °C, approximately double the reduction achieved in LCZ8 (0.8 °C), which has large low-rise buildings. This is because LCZ2 has a higher roof/surface area ratio and consequently a larger net radiation than LCZ8. It is interesting to note that although there is no change in albedo for LCZ6 and LCZ8, we can appreciate a small temperature reduction given their proximity to and the buffering effects of LCZ2 and LCZ8. This is not the case for LCZ9 (sparsely built) cells (also with no change in albedo), which are farther away from LCZ2 and LCZ8.

7.2. How the temperature reduction scenarios affect the energy balance

The energy balance of the urban areas in the study region is the sum of the net radiation received and the various forms of energy emitted in the form of ground heat, latent heat, and sensible heat, which includes anthropogenic heat fluxes herein. The various mitigation strategies reduce the sensible heat flux in various ways, with an overall net effect of air temperature reduction. Fig. 8 shows the difference in the average daily profile between the reference case and each scenario for the various components of the surface

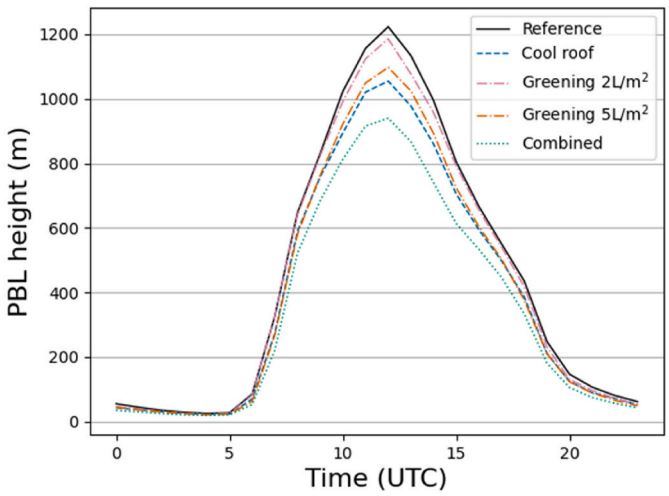

Fig. 7. Urban boundary layer height for the different scenarios and the reference case averaged over the three days most intense days of the heat wave 4/06/2015 to 6/06/2015.

energy balance over the urban area of the AMB (represented in gray shades in Fig. 1b).

In the scenario with increased rooftop albedo, we observe a decrease in the net radiation during the daylight hours, with a reduction peak of 77 W/m^2 at 12:00 UTC corresponding to an increase in roof reflectivity. This increase in reflectivity decreases the absorption of shortwave radiation, consequently decreasing the surface temperature. We conclude that the decrease in the net radiation flux reduces the sensible heat flux between the surface and the atmosphere, with a reduction peak of 88 W/m^2 at 12:00 UTC. However, this scenario also indirectly affects the latent heat component of the energy balance, which decreases by 5 W/m^2 at 12:00 UTC, most likely due to more surface moisture limiting evapotranspiration, either directly from the soil or from transpiration from plants. The reduction in the sensitive heat flow from the roofs of buildings limits the convective growth of the planetary boundary layer (PBL), which increases until afternoon by the vertical movements of hot air from the surface when the sky is clear and there are periods of high radiation. The less developed PBL during daytime hours (between 7:00 UTC and 18:00 UTC, see Fig. 7) results in a lower mixing height and a uniform distribution of the potential temperature and humidity, consequently slightly increasing the surface humidity. Finally, the reduction in the roof surface temperature means that less energy is transferred in the form of heat to the innermost layers of urban materials, which is reflected in the peak reduction in ground heat flux (28 W/m^2 at 8:00 UTC).

A different cooling mechanism is seen for the greening scenario and the various irrigation schemes. More availability of water in the surface layers in addition to more vegetation increase evapotranspiration by direct evaporation from the soil and transpiration through vegetation, increasing the latent heat flows, with peaks of 12.5 W/m^2 at 10:00 UTC and 78 W/m^2 at 13:00 UTC for the two irrigation schemes (2 and 5 L/m^2 day, respectively). Therefore, there is an increase in the latent heat flux to the detriment of the sensible heat and ground heat flux, causing a decrease in the daytime and nighttime temperatures. The lower irrigation scheme (2 L/m^2 day) results in a greater decrease in the ground heat flux (−7.6 W/m^2) at a time with a greater latent heat increase and zero change in the sensible heat flux, suggesting that the greatest impact on temperature is seen during the nighttime hours instead of during the day, as less heat is retained in the innermost layers of the soil to be later released into the atmosphere. It should also be noted that in these two scenarios, there is a slight increase in the flow of net radiation, caused in part by the decrease in albedo when the soil is moist and due to the decrease in the surface temperature of the soil, which increases the balance of the longwave radiation exchange.

Finally, the combined scenario shows a reduction in temperature proportional to the sum of the two scenarios mentioned above,

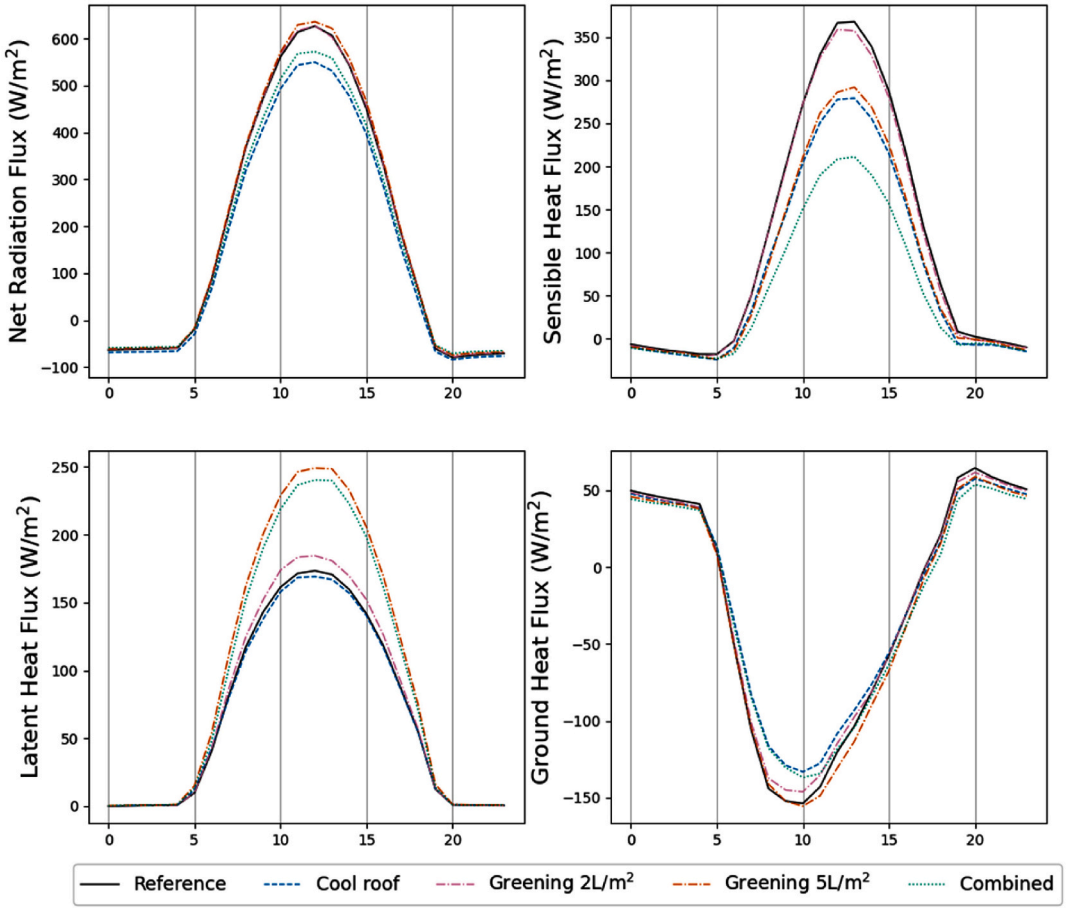

Fig. 8. Daily profiles of various components of the surface energy balance (a) net radiation flux; (b) sensible heat flux; (c) latent heat flux (d) ground heat flux averaged over the entire AMB and the three intense days of the heat wave 4/06/2015 to 6/06/2015.

because these two mechanisms affect the different surface processes in a similar way (i.e., less shortwave radiation absorption and more evapotranspiration). This is illustrated by Fig. 8a, where we see that the lowest sensible heat flux for the combined scenario (158 W/m^2 at 12:00 UTC) corresponds to the period of maximum solar insolation. However, there are certain hours when the temperature reduction mechanisms of the various mitigation strategies limit each other, albeit to a small extent. We observe a higher net radiation flux for the combined scenario than for the cool roof scenario during the period with maximum solar radiation (12:00 UTC) (see Fig. 8a) due to the aforementioned processes that occur in the greening scenarios: a greater absorption of short radiation due to a slight decrease in albedo and a decrease in the longwave emission due to a decrease in surface temperature. We also observe a lower latent heat flux for the combined scenario than for the greening scenario with high irrigation (5 L/m^2·day, see Fig. 8b) due to the decrease in the PBL height, which reaches a maximum mean difference of 283 m and consequently increases the surface moisture limiting evapotranspiration (Fig. 7).

The anthropogenic heat flux of the simulations is limited to the heat produced by air conditioning units and excludes all the heat produced from industrial processes or vehicle use. The cooling effect of the scenarios results in less use of air conditioning (AC), which consequently further reduces temperatures, because less anthropogenic heat is released to the atmosphere from the AC units. This heat flux is an order of magnitude lower than the rest of the fluxes and does not contribute much to the overall energy balance. However, the energy savings for the city are significant. The simulation of the combined scenario estimates a 26% reduction in electricity consumption due to AC usage at 16:00 UTC (see Fig. S6 in the Supporting Information). When we average these reductions for the entire urban area and for the three hottest days of the HW, we estimate electricity reductions of 25%, 16%, and 9–10% for the combined, cool roof, and greening scenarios, respectively, based on the electricity consumption estimated for the reference scenario (211 GWh).

8. Conclusions

The overall aim of this study is to advance our knowledge of the design and efficacy of heat wave mitigation strategies by more accurately representing the heterogeneity of urban land use in models to better simulate land-atmosphere interactions at the city scale. To do so, we use eleven urban local climate zone (LCZ) classes and fine-resolution data, characterizing the urban and vegetation fractions of the study region in an attempt to more accurately resolve the surface heterogeneity effects of the urban fabric using the WRF BEP + BEM model. We choose the Metropolitan Area of Barcelona during the heat wave of July 2015 as a case study with which to validate the model, perform the urban parameterization (with RMSE errors below 1.5 °C and a positive BIAS below 0.5 °C) and simulate three mitigation strategies: 1) the implementation of cool roofs, increasing the albedo to 0.85 for LCZ's that make up 20% of the urban area, 2) incrementing the urban green space by an additional 255.64 ha, according to the proposal of the Master Urban Plan for 2030, with two different irrigation schemes (2 and 5 L/m^2 day), and 3) a combination of the first two complementary mitigation strategies. We find that cool roofs reduce temperatures mostly during the day, while the additional green areas help to moderate temperatures evenly during the day and at night. However, when irrigation is increased from 2 to 5 L/m^2 day, the temperature reduction potential during the day is intensified due to the cooling effect of more evapotranspiration. The combined scenario (cool roofs and more green areas with augmented irrigation) leads to a reduction in the temperature proportional to the sum of the two scenarios, because the two cooling mechanisms affect different surface processes and are generally complementary.

Incrementing the albedo of the roofs resulted in the highest temperature reductions, especially during the day, when the net radiation was largest, with average reductions of 0.67 °C and a maximum reduction of 3.83 °C at 13:00 UTC. The maximum reduction potential is found for LCZ's 1 and 2, since they have the most roof surface area. Cool roofs are not as effective in reducing temperatures at night, when there is no shortwave radiation, and the cooling effect occurs mostly because less heat accumulates in the buildings during the day. Incrementing the urban green areas and maintaining the current irrigation scheme has a moderate impact, with an average daytime reduction of 0.15 °C and a maximum reduction of 1.70 °C at 11:00 UTC. The thermal regulation potential of the green scenario is greatly intensified when irrigation is increased, resulting in an average daytime reduction of 0.61 °C, four times more than that of the less irrigated scenario, and covering a more extensive area of the AMB due to the spreading effect of the daytime sea breezes. The thermal regulation potential of the combined scenario has the greatest effect over the AMB and the highest impact, with an average daytime reduction of 1.26 °C and a maximum reduction of 4.73 °C at 13:00 UTC in LCZs 1 and 2 and urban parks. In conclusion, this study exemplifies how such urban modeling efforts can aid city-level decision-makers in best strategizing urban planning to counteract the impacts of heat waves, which are foreseen to increase due to global climate change and the intensification of urbanization rates.

Declaration of Competing Interest

The authors declare that they have no known competing financial interests or personal relationships that could have appeared to influence the work reported in this paper.

Acknowledgements

This work has been made possible thanks to the financial support of the ERC Consolidator Integrated System Analysis of Urban Vegetation and Agriculture (818002-URBAG). The authors would also like to thank the support of the Spanish Ministry of Science, Innovation and Universities, through the “Maria de Maeztu” programme for Units of Excellence (CEX2019-000940-M). The authors thankfully acknowledge the computer resources at PICASSO and the technical support provided by the Universidad de Málaga (RES-AECT-2020-2-0004). The authors further wish to thank Annalisa Jacoli and Jacob Cirera of the Pla Director Urbanistic of the Metropolitan Area of Barcelona and the Meteorological Service of Catalonia for the data used.

Appendix A. Supplementary data

Supplementary data to this article can be found online at https://doi.org/10.1016/j.uclim.2021.100863.

References

Ackerman, S., Knox, J., 2012. Meteorology: understanding the atmosphere. In: Jones and Bartlett Learning, 3rd ed, p. 578.

Akbari, H., Pomerantz, M., Taha, H., 2001. Cool surfaces and shade trees to reduce energy use and improve air quality in urban areas. Sol. Energy 70. https://doi.org/10.1016/S0038-092X(00)00089-X.

Ajuntament de Barcelona, 2013. Guidelines for Irrigation: A practical guide for the irrigation of green areas of Barcelona. Medi Ambient i Serveis Urbans. https://ajuntament.barcelona.cat/ecologiaurbana/sites/default/files/Manual-Reg-Parcs-Jardins.pdf (Last accessed May 2021).

Akbari, H., Menon, S., Rosenfeld, A., 2009. Global cooling: increasing world-wide urban albedos to offset CO 2. Clim. Chang. 94 https://doi.org/10.1007/s10584-008-9515-9.

Alamús, R., Pérez, F., Pipia, L., Corbera, J., 2018. Urban sustainable ecosystems assessment through airborne earth observation: lessons learned. In: International Archives of the Photogrammetry, Remote Sensing and Spatial Information Sciences - ISPRS Archives. https://doi.org/10.5194/isprs-archives-XLII-1-5-2018.

Altava, V., Barrera, A., Amaro, J., Cunillera, J., Sairouni, A., 2015. Generació d'escenaris climàtics futurs regionalitzats a molt alta resolució (1km) per a l'Àrea Metropolitana de Barcelona (Projecte ESAMB). In: Direcció de Serveis Ambientals de l'AMB (Ed.), METROBS 2015.

Arnfield, A.J., 2003. Two decades of urban climate research: a review of turbulence, exchanges of energy and water, and the urban heat island. Int. J. Climatol. 23 https://doi.org/10.1002/joc.859.

Ballester, J., Douville, H., Chauvin, F., 2009. Present-day climatology and projected changes of warm and cold days in the CNRM-CM3 global climate model. Clim. Dyn. 32 https://doi.org/10.1007/s00382-008-0371-0.

Barriopedro, D., Fischer, E.M., Luterbacher, J., Trigo, R.M., García-Herrera, R., 2011. The hot summer of 2010: redrawing the temperature record map of Europe. Science (80-.) 332. https://doi.org/10.1126/science.1201224.

Bechtel, B., Alexander, P.J., Böhner, J., Ching, J., Conrad, O., Feddema, J., Mills, G., See, L., Stewart, I., 2015. Mapping local climate zones for a worldwide database of the form and function of cities. ISPRS Int. J. Geo-Inform. 4 https://doi.org/10.3390/ijgi4010199.

Bougeault, P., Lacarrere, P., 1989. Parameterization of orography-induced turbulence in a mesobeta-scale model. Mon. Weather Rev. 117. https://doi.org/10.1175/1520-0493(1989)117<1872:POOITI>2.0.CO;2.

Bowler, D.E., Buyung-Ali, L., Knight, T.M., Pullin, A.S., 2010. Urban greening to cool towns and cities: a systematic review of the empirical evidence. Landsc. Urban Plan. https://doi.org/10.1016/j.landurbplan.2010.05.006.

Bretz, S.E., Akbari, H., 1997. Long-term performance of high-albedo roof coatings. Energy Build. 25 https://doi.org/10.1016/s0378-7788(96)01005-5.

Brousse, O., Martilli, A., Foley, M., Mills, G., Bechtel, B., 2016. WUDAPT, an efficient land use producing data tool for mesoscale models? Integration of urban LCZ in WRF over Madrid. Urban Clim. 17 https://doi.org/10.1016/j.uclim.2016.04.001.

Cadenasso, M.L., Pickett, S.T.A., Schwarz, K., 2007. Spatial heterogeneity in urban ecosystems: Reconceptualizing land cover and a framework for classification. Front. Ecol. Environ. https://doi.org/10.1890/1540-9295(2007)5[80:SHIUER]2.0.CO;2.

Campra, P., 2011. Global and local effect of increasing land surface Albedo as a geo-engineering Adaptation/Mitigation option: a study case of Mediterranean greenhouse farming. In: Climate Change - Research and Technology for Adaptation and Mitigation. https://doi.org/10.5772/23286.

Campra, P., Garcia, M., Canton, Y., Palacios-Orueta, A., 2008. Surface temperature cooling trends and negative radiative forcing due to land use change toward greenhouse farming in southeastern Spain. J. Geophys. Res. Atmos. 113 https://doi.org/10.1029/2008JD009912.

Chen, F., Dudhia, J., 2001. Coupling and advanced land surface-hydrology model with the Penn State-NCAR MM5 modeling system. Part I: model implementation and sensitivity. Mon. Weather Rev. 129 https://doi.org/10.1175/1520-0493(2001)129<0569:CAALSH>2.0.CO;2.

Chen, F., Manning, K.W., Lemone, M.A., Trier, S.B., Alfieri, J.G., Roberts, R., Blanken, P.D., 2007. Description and evaluation of the characteristics of the NCAR high-resolution land data assimilation system. J. Appl. Meteorol. Climatol. 46 (6), 694–713. https://doi.org/10.1175/JAM2463.1.

De Ridder, K., Lauwaet, D., Maiheu, B., 2015. UrbClim - a fast urban boundary layer climate model. Urban Clim. 12 https://doi.org/10.1016/j.uclim.2015.01.001.

Demuzere, M., Orru, K., Heidrich, O., Olazabal, E., Geneletti, D., Orru, H., Bhave, A.G., Mittal, N., Feliu, E., Faehnle, M., 2014. Mitigating and adapting to climate change: multi-functional and multi-scale assessment of green urban infrastructure. J. Environ. Manag. 146 https://doi.org/10.1016/j.jenvman.2014.07.025.

Eliasson, I., 1996. Urban nocturnal temperatures, street geometry and land use. In: Atmospheric Environment. https://doi.org/10.1016/1352-2310(95)00033-X.

Fallmann, J., Emeis, S., Suppan, P., 2013. Mitigation of urban heat stress -a modelling case study for the area of Stuttgart. Erde 144. https://doi.org/10.12854/erde-144-15.

Feyisa, G.L., Dons, K., Meilby, H., 2014. Efficiency of parks in mitigating urban heat island effect: an example from Addis Ababa. Landsc. Urban Plan. 123 https://doi.org/10.1016/j.landurbplan.2013.12.008.

Gago, E.J., Roldan, J., Pacheco-Torres, R., Ordóñez, J., 2013. The city and urban heat islands: a review of strategies to mitigate adverse effects. Renew. Sust. Energ. Rev. https://doi.org/10.1016/j.rser.2013.05.057.

Geletič, J., Lehnert, M., Dobrovolný, P., 2016. Land surface temperature differences within local climate zones, based on two central European cities. Remote Sens. 8 https://doi.org/10.3390/rs8100788.

Getter, K.L., Rowe, D.B., 2006. The role of extensive green roofs in sustainable development. HortScience 41. https://doi.org/10.21273/hortsci.41.5.1276.

Gilabert, J., Deluca, A., Lauwaet, D., Ballester, J., Corbera, J., Llasat, M.C., 2021. Assessing heat exposure to extreme temperatures in urban areas using the local climate zones classification. Nat. Hazards Earth Syst. Sci. 21 (1), 375–391. https://doi.org/10.5194/nhess-21-375-2021.

Giorgi, F., 2006. Climate change hot-spots. Geophys. Res. Lett. 33 https://doi.org/10.1029/2006GL025734.

González, M.Á., Arasa, R., Gámez, P., Picanyol, M., Campra, P., 2019. Effects of increasing the surface reflectance over air quality levels using WRF-BEM/AEMM/CMAQ: Application over the city of Madrid. Int. J. Environ. Poll. https://doi.org/10.1504/IJEP.2019.101841.

Guarino, M.V., Martilli, A., Di Sabatino, S., Leo, L.S., 2014. Modelling the urban boundary-layer over a typical mediterranean city using WRF: assessment of UHI and thermal comfort. In: American Society of Mechanical Engineers, Fluids Engineering Division (Publication) FEDSM. https://doi.org/10.1115/FEDSM2014-21572.

Guerreiro, S.B., Dawson, R.J., Kilsby, C., Lewis, E., Ford, A., 2018. Future heat-waves, droughts and floods in 571 European cities. Environ. Res. Lett. 13 https://doi.org/10.1088/1748-9326/aaaad3.

Habitat, U., 2013. State of the world's Cities 2012/2013: Prosperity of Cities, State of the World's Cities 2012/2013: Prosperity of Cities. https://doi.org/10.4324/9780203756171.

Hersbach, H., Bell, B., Berrisford, P., Hirahara, S., Horányi, A., Muñoz-Sabater, J., Nicolas, J., Peubey, C., Radu, R., Schepers, D., Simmons, A., Soci, C., Abdalla, S., Abellan, X., Balsamo, G., Bechtold, P., Biavati, G., Bidlot, J., Bonavita, M., De Chiara, G., Dahlgren, P., Dee, D., Diamantakis, M., Dragani, R., Flemming, J., Forbes, R., Fuentes, M., Geer, A., Haimberger, L., Healy, S., Hogan, R.J., Hólm, E., Janisková, M., Keeley, S., Laloyaux, P., Lopez, P., Lupu, C., Radnoti, G., de Rosnay, P., Rozum, I., Vamborg, F., Villaume, S., Thépaut, J.N., 2020. The ERA5 global reanalysis. Q. J. R. Meteorol. Soc. 146 https://doi.org/10.1002/qj.3803.

Holtanová, E., Valeriánová, A., Crhová, L., Racko, S., 2014. Heat wave of august 2012 in the Czech Republic: comparison of two approaches to assess high temperature event. Stud. Geophys. Geod. 59 https://doi.org/10.1007/s11200-014-0805-6.

Hong, S.-Y., Lim, J.-O. Jade, 2006. The WRF single-moment 6-class microphysics scheme (WSM6). Asia-Pac. J. Atmos. Sci. 42 (2), 129–151.

Hoy, A., Hänsel, S., Skalak, P., Ustrnul, Z., Bochníček, O., 2017. The extreme European summer of 2015 in a long-term perspective. Int. J. Climatol. 37 https://doi.org/10.1002/joc.4751.

Huler, S., 2004. Defining the Wind: the Beaufort Scale, and How a Nineteenth-century Admiral Turned Science into Poetry. Crown Publishing Group, Three Rivers Press, New York (290 p.) ISBN 1-4000-4885-0.
Iacono, M.J., Delamere, J.S., Mlawer, E.J., Shephard, M.W., Clough, S.A., Collins, W.D., 2008. Radiative forcing by long-lived greenhouse gases: calculations with the AER radiative transfer models. J. Geophys. Res. Atmos. 113 https://doi.org/10.1029/2008JD009944.
Ingole, V., Marí-Dell'Olmo, M., Deluca, A., Quijal, M., Borrell, C., Rodríguez-Sanz, M., Achebak, H., Lauwaet, D., Gilabert, J., Murage, P., Hajat, S., Basagaña, X., Ballester, J., 2020. Spatial variability of heat-related mortality in Barcelona from 1992-2015: A case crossover study design. Int. J. Environ. Res. Public Health 17. https://doi.org/10.3390/ijerph17072553.
Institute Cartographic and Geological of Catalonia (ICGC), 2019. LiDAR Data. https://www.icgc.cat/es/Descargas/Elevaciones/Datos-lidar (accessed 16 July 2019).
Jacobs, S.J., Gallant, A.J.E., Tapper, N.J., Li, D., 2018. Use of cool roofs and vegetation to mitigate urban heat and improve human thermal stress in Melbourne, Australia. J. Appl. Meteorol. Climatol. 57 https://doi.org/10.1175/JAMC-D-17-0243.1.
Jaffal, I., Ouldboukhitine, S.E., Belarbi, R., 2012. A comprehensive study of the impact of green roofs on building energy performance. Renew. Energy 43. https://doi.org/10.1016/j.renene.2011.12.004.
Jandaghian, Z., Touchaei, A.G., Akbari, H., 2018. Sensitivity analysis of physical parameterizations in WRF for urban climate simulations and heat island mitigation in Montreal. Urban Clim. 24, 577–599.
Jiménez-Esteve, B., Udina, M., Soler, M.R., Pepin, N., Miró, J.R., 2018. Land use and topography influence in a complex terrain area: a high resolution mesoscale modelling study over the eastern Pyrenees using the WRF model. Atmos. Res. 202, 49–62.
Kain, J.S., Kain, J., 2004. The Kain - Fritsch convective parameterization: an update. J. Appl. Meteorol. 43 https://doi.org/10.1175/1520-0450(2004)043<0170:TKCPAU>2.0.CO;2.
Kyselý, J., 2010. Recent severe heat waves in Central Europe: how to view them in a long-term prospect? Int. J. Climatol. 30 https://doi.org/10.1002/joc.1874.
Lhotka, O., Kyselý, J., 2015. Characterizing joint effects of spatial extent, temperature magnitude and duration of heat waves and cold spells over Central Europe. Int. J. Climatol. 35 https://doi.org/10.1002/joc.4050.
Li, D., Bou-Zeid, E., 2013. Synergistic interactions between urban heat islands and heat waves: the impact in cities is larger than the sum of its parts. J. Appl. Meteorol. Climatol. 52 https://doi.org/10.1175/JAMC-D-13-02.1.
Li, X.X., Norford, L.K., 2016. Evaluation of cool roof and vegetations in mitigating urban heat island in a tropical city, Singapore. Urban Clim. 16 https://doi.org/10.1016/j.uclim.2015.12.002.
Li, J.F., Wai, O.W.H., Li, Y.S., Zhan, J.M., Ho, Y.A., Li, J., Lam, E., 2010. Effect of green roof on ambient CO2 concentration build. Environ. 45, 2644–2651.
Li, D., Bou-Zeid, E., Oppenheimer, M., 2014. The effectiveness of cool and green roofs as urban heat island mitigation strategies. Environ. Res. Lett. 9 https://doi.org/10.1088/1748-9326/9/5/055002.
Li, H., Wolter, M., Wang, X., Sodoudi, S., 2018. Impact of land cover data on the simulation of urban heat island for Berlin using WRF coupled with bulk approach of Noah-LSM. Theor. Appl. Climatol. 134 https://doi.org/10.1007/s00704-017-2253-z.
Liang, S., 2001. Narrowband to broadband conversions of land surface albedo I algorithms. Remote Sens. Environ. 76 https://doi.org/10.1016/S0034-4257(00)00205-4.
Lindberg, F., Grimmond, C.S.B., Gabey, A., Huang, B., Kent, C.W., Sun, T., Theeuwes, N.E., Järvi, L., Ward, H.C., Capel-Timms, I., Chang, Y., Jonsson, P., Krave, N., Liu, D., Meyer, D., Olofson, K.F.G., Tan, J., Wästberg, D., Xue, L., Zhang, Z., 2018. Urban multi-scale environmental predictor (UMEP): an integrated tool for city-based climate services. Environ. Model. Softw. 99 https://doi.org/10.1016/j.envsoft.2017.09.020.
Luber, G., McGeehin, M., 2008. Climate change and extreme heat events. Am. J. Prev. Med. https://doi.org/10.1016/j.amepre.2008.08.021.
Martilli, A., 2002. Numerical study of urban impact on boundary layer structure: sensitivity to wind speed, urban morphology, and rural soil moisture. J. Appl. Meteorol. 41 https://doi.org/10.1175/1520-0450(2002)041<1247:NSOUIO>2.0.CO;2.
Martilli, A., Brousse, O., Ching, J., . Urbanized WRF modeling using WUDAPT(1). Http://Www.Wudapt.Org/Resources/, pp. 1–8.
Meteorological Service of Catalonia (SMC), 2015. Monthly weather bulletin July 2015. Departament de Territori i Sostenibilitat. https://static-m.meteo.cat/wordpressweb/wp-content/uploads/2015/06/08111706/Butlletˆ%C3%AD-juliol15.pdf (Last accessed May 2021).
Metropolitan Urban Master Plan, 2019. PDU https:\\urbanisme.amb.cat\en\home (accessed: 23 July 2019).
Millstein, D., Menon, S., 2011. Regional climate consequences of large-scale cool roof and photovoltaic array deployment. Environ. Res. Lett. 6 https://doi.org/10.1088/1748-9326/6/3/034001.
Moreno-garcia, M.C., 1994. Intensity and form of the urban heat island in Barcelona. Int. J. Climatol. 14 https://doi.org/10.1002/joc.3370140609.
Morini, E., Touchaei, A.G., Castellani, B., Rossi, F., Cotana, F., 2016. The impact of albedo increase to mitigate the urban heat island in Terni (Italy) using the WRF model. Sust. 999 https://doi.org/10.3390/su8100999.
Morini, E., Castellani, B., De Ciantis, S., Andreini, E., Rossi, F., 2018. Planning for cooler urban canyons: comparative analysis of the influence of façades reflective properties on urban canyon thermal behavior. Sol. Energy 162. https://doi.org/10.1016/j.solener.2017.12.064.
Ndossi, M.I., Avdan, U., 2016. Application of open source coding technologies in the production of land surface temperature (LST) maps from Landsat: a PyQGIS plugin. Remote Sens. 8 https://doi.org/10.3390/rs8050413.
Oke, T.R., 1982. The energetic basis of the urban heat island. Q. J. R. Meteorol. Soc. 108 https://doi.org/10.1002/qj.49710845502.
Oleson, K.W., Bonan, G.B., Feddema, J., 2010. Effects of white roofs on urban temperature in a global climate model. Geophys. Res. Lett. 37 https://doi.org/10.1029/2009GL042194.
Pachauri, R.K., Meyer, L.A., 2015. IPCC 2014, Climate Change 2014: Synthesis Report. Contribution of Working Groups I, II and III to the Fifth Assessment Report of the Intergovernmental Panel on Climate Change. IPCC.
Papangelis, G., Tombrou, M., Dandou, A., Kontos, T., 2012. An urban "green planning" approach utilizing the weather research and forecasting (WRF) modeling system. A case study of Athens, Greece. Landsc. Urban Plan. 105 https://doi.org/10.1016/j.landurbplan.2011.12.014.
Pappaccogli, G., Giovannini, L., Cappelletti, F., Zardi, D., 2017. Sensitivity of WRF/urban simulations to urban morphology parameters: A case study in the city of bolzano. In: Building Simulation Applications.
Qiu, G. Yu, Li, H. Yong, Zhang, Q. Tao, Chen, W., Liang, X. Jian, Li, X. Ze, 2013. Effects of evapotranspiration on mitigation of urban temperature by vegetation and urban agriculture. J. Integr. Agric. https://doi.org/10.1016/S2095-3119(13)60543-2.
Red Eléctrica de España (REE), 2016. Informe del Sistema Eléctrico Español 2015. Ed. Departamento de Comunicación e Imagen Corporativa de Red Eléctrica. https://www.ree.es/sites/default/files/downloadable/inf_sis_elec_ree_2015.pdf.
Ribeiro, I., Martilli, A., Falls, M., Zonato, A., Villalba, G., 2021. Highly resolved WRF-BEP/BEM simulations over Barcelona urban area with LCZ. Atmos. Res. 248 https://doi.org/10.1016/j.atmosres.2020.105220.
Rothfusz, L.P., Headquarters, N.S.R., 1990. The heat index equation (or, more than you ever wanted to know about heat index). National Oceanic and Atmospheric Administration, National Weather Service, Office of Meteorology, Fort Worth, Texas, p. 9023.
Rowe, D.B., Getter, K.L., 2015. Green Roofs and Garden Roofs. https://doi.org/10.2134/agronmonogr55.c19.
Salamanca, F., Martilli, A., 2010. A new Building Energy Model coupled with an Urban Canopy Parameterization for urban climate simulations-part II. Validation with one dimension off-line simulations. Theor. Appl. Climatol. 99. https://doi.org/10.1007/s00704-009-0143-8.
Salamanca, F., Krpo, A., Martilli, A., Clappier, A., 2010. A new building energy model coupled with an urban canopy parameterization for urban climate simulations-part I. formulation, verification, and sensitivity analysis of the model. Theor. Appl. Climatol. 99 https://doi.org/10.1007/s00704-009-0142-9.
Salamanca, F., Martilli, A., Tewari, M., Chen, F., 2011. A study of the urban boundary layer using different urban parameterizations and high-resolution urban canopy parameters with WRF. J. Appl. Meteorol. Climatol. 50 https://doi.org/10.1175/2010JAMC2538.1.
Salamanca, F., Martilli, A., Yagüe, C., 2012. A numerical study of the urban Heat Island over Madrid during the DESIREX (2008) campaign with WRF and an evaluation of simple mitigation strategies. Int. J. Climatol. 32 https://doi.org/10.1002/joc.3398.
Santamouris, M., 2014. Cooling the cities - a review of reflective and green roof mitigation technologies to fight heat island and improve comfort in urban environments. Sol. Energy 103. https://doi.org/10.1016/j.solener.2012.07.003.

Schneidereit, A., Schubert, S., Vargin, P., Lunkeit, F., Zhu, X., Peters, D.H.W., Fraedrich, K., 2012. Large-scale flow and the long-lasting blocking high over Russia: summer 2010. Mon. Weather Rev. 140 https://doi.org/10.1175/MWR-D-11-00249.1.

Sharma, A., Fernando, H.J.S., Hellmann, J., Chen, F., 2014. Sensitivity of WRF model to urban parameterizations, with applications to Chicago metropolitan urban heat island. In: American Society of Mechanical Engineers, Fluids Engineering Division (Publication) FEDSM. https://doi.org/10.1115/FEDSM2014-21292.

Sharma, A., Conry, P., Fernando, H.J.S., Hamlet, A.F., Hellmann, J.J., Chen, F., 2016. Green and cool roofs to mitigate urban heat island effects in the Chicago metropolitan area: evaluation with a regional climate model. Environ. Res. Lett. 11 https://doi.org/10.1088/1748-9326/11/6/064004.

Skamarock, W.C., Klemp, J.B., Dudhia, J., Gill, D.O., Liu, Z., Berner, J., Wang, W., Powers, J.G., Duda, M.G., Barker, D.M., Huang, X.-Y., 2019. A Description of the Advanced Research WRF Version 4. NCAR Tech. Note NCAR/TN-556+STR, p. 145. https://doi.org/10.5065/1dfh-6p97.

Smid, M., Russo, S., Costa, A.C., Granell, C., Pebesma, E., 2019. Ranking European capitals by exposure to heat waves and cold waves. Urban Clim. 27 https://doi.org/10.1016/j.uclim.2018.12.010.

Soler, M.R., Arasa, R., Merino, M., Olid, M., Ortega, S., 2011. Modelling local sea-breeze flow and associated dispersion patterns over a coastal area in north-east spain: a case study. Boundary-Layer Meteorol. 140. https://doi.org/10.1007/s10546-011-9599-z.

Stewart, I.D., Oke, T.R., 2012. Local climate zones for urban temperature studies. Bull. Am. Meteorol. Soc. 93 https://doi.org/10.1175/BAMS-D-11-00019.1.

Synnefa, A., Santamouris, M., 2012. Advances on Technical, Policy and Market Aspects of Cool Roof Technology in Europe: The Cool Roofs Project, in: Energy and Buildings. https://doi.org/10.1016/j.enbuild.2011.11.051.

Synnefa, A., Dandou, A., Santamouris, M., Tombrou, M., Soulakellis, N., 2008. On the use of cool materials as a heat island mitigation strategy. J. Appl. Meteorol. Climatol. 47 https://doi.org/10.1175/2008JAMC1830.1.

Tan, J., Zheng, Y., Tang, X., Guo, C., Li, L., Song, G., Zhen, X., Yuan, D., Kalkstein, A.J., Li, F., Chen, H., 2010. The urban heat island and its impact on heat waves and human health in Shanghai. Int. J. Biometeorol. 54 https://doi.org/10.1007/s00484-009-0256-x.

United Nations, 2015. World Population Prospects: The 2015 Revision. United Nations Economic and Social Affairs.

United States Geological Survey (USGS), 2019. Earth Explorer. https://earthexplorer.usgs.gov/ (accessed 16 July 2019).

Upmanis, H., Eliasson, I., Lindqvist, S., 1998. The influence of green areas on nocturnal temperatures in a high latitude city (Goteborg, Sweden). Int. J. Climatol. 18 https://doi.org/10.1002/(SICI)1097-0088(199805)18:6<681::AID-JOC289>3.0.CO;2-L.

Vermote, E., Justice, C., Claverie, M., Franch, B., 2016. Preliminary analysis of the performance of the Landsat 8/OLI land surface reflectance product. Remote Sens. Environ. 185 https://doi.org/10.1016/j.rse.2016.04.008.

Ward, K., Lauf, S., Kleinschmit, B., Endlicher, W., 2016. Heat waves and urban heat islands in Europe: a review of relevant drivers. Sci. Total Environ. 569–570. https://doi.org/10.1016/j.scitotenv.2016.06.119.

Yang, J., Wang, Z.H., Kaloush, K.E., 2015. Environmental impacts of reflective materials: is high albedo a “silver bullet” for mitigating urban heat island? Renew. Sust. Energ. Rev. https://doi.org/10.1016/j.rser.2015.03.092.

Yu, Z., Guo, X., Zeng, Y., Koga, M., Vejre, H., 2018. Variations in land surface temperature and cooling efficiency of green space in rapid urbanization: the case of Fuzhou city, China. Urban For. Urban Green. 29 https://doi.org/10.1016/j.ufug.2017.11.008.

Yuan, F., Bauer, M.E., 2007. Comparison of impervious surface area and normalized difference vegetation index as indicators of surface urban heat island effects in Landsat imagery. Remote Sens. Environ. 106. https://doi.org/10.1016/j.rse.2006.09.003.

Zinzi, M., Agnoli, S., 2012. Cool and green roofs. An energy and comfort comparison between passive cooling and mitigation urban heat island techniques for residential buildings in the Mediterranean region. Energy Build. https://doi.org/10.1016/j.enbuild.2011.09.024.

Zonato, A., Martilli, A., Di Sabatino, S., Zardi, D., Giovannini, L., 2020. Evaluating the performance of a novel WUDAPT averaging technique to define urban morphology with mesoscale models. Urban Clim. 31 https://doi.org/10.1016/j.uclim.2020.100584.